SYNOVIAL FLUID PROFILE DICTATES NANOPARTICLE UPTAKE INTO CARTILAGE - IMPLICATIONS OF THE PROTEIN CORONA FOR NOVEL ARTHRITIS TREATMENTS

Ula von Mentzer[1], Tilia Selldén[1], Loise Råberg[1], Gizem Erensoy[1], Anna-Karin Hultgård Ekwall[2,3], Alexandra Stubelius[1,]*

[1]*Division of Chemical Biology, Department of Biology and Biological Engineering, Chalmers University of Technology, Gothenburg, Sweden.*

[2]*The Rheumatology Clinic, Sahlgrenska University Hospital, Gothenburg, Sweden.*

[3]*Department of Rheumatology and Inflammation Research, Institute of Medicine, Sahlgrenska Academy, University of Gothenburg, Gothenburg, Sweden.*

*Corresponding author: Alexandra Stubelius, Alexandra.stubelius@chalmers.se

Postal address: Kemivägen 10, 41296 Gothenburg, Sweden

Abstract

Objective

Drug delivery strategies for joint diseases need to overcome the negatively charged cartilage matrix. Previous studies have extensively investigated particle approaches to increase uptake efficiency by harnessing the anionic charge of the cartilage, but have neglected to address potential interactions with the protein-rich biological environment of the joint space. We aimed to evaluate the effects of hard protein coronas derived from osteoarthritis (OA) and rheumatoid arthritis (RA) patient synovial fluids as well as the commonly used fetal calf serum (FCS) on nanoparticle (NP) uptake into tissues and cells.

Methods

We developed an NP panel with varying PEGylation and incubated them with synovial fluid from either OA, RA patients or FCS. We evaluated the effects of the formed NP-biocorona complex uptake into the porcine articular cartilage explants and in chondrocytes and monocytes. Proteins composing hard biocoronas were identified using a quantitative proteomics approach.

Results

Formed biocoronas majorly impacted NP uptake into cartilage tissue and dictated their uptake in chondrocytes and monocytes. The most suitable NP for potential OA applications was identified. A variety of proteins that were found on all NPs, irrespective of surface modifications. NP-, and protein-specific differences were also observed between the groups, and candidate proteins were identified that could account for the observed differences.

Conclusions

This study demonstrates the impact of protein coronas from OA and RA patient synovial fluids on NP uptake into cartilage, emphasizing the importance of biological

39 microenvironment considerations for successful translation of drug delivery vehicles into
40 clinics.

41

42 Keywords: Drug delivery; cartilage, synovial fluid, arthritis, protein corona

43

INTRODUCTION

A major obstacle for therapies targeting joint diseases has been to reach the chondrocytes deeply embedded in the extracellular cartilage matrix (ECM). This dense, avascular, and aneural network of large and highly negatively charged macromolecules poses a physical barrier for reaching the cells. Retention in the synovial space is crucial to increase therapeutic uptake into tissues and avoid clearance[1]. Recent advancements in intra-articular drug delivery have leveraged both small sizes and electrostatic interactions with the anionic ECM[2,3]. It is well known that micro- and nanoscale drug delivery approaches are immediately subjected to the high abundance of host-derived biological components such as proteins, carbohydrates, and lipids[4]. These bioactive components can alter the size and surface composition of the particles and equip them with a distinct biological identity, in turn, dictating their physiological and therapeutic outcomes[4,5]. For instance, studies on systemic administration have shown that just a simple change from blood plasma to serum had a profound difference in both protein corona composition and nanoparticle (NP) fate, demonstrating the importance of selecting the appropriate environment to account for in vivo settings[6]. Yet so far, no studies have addressed the potential effect of the OA and RA patient synovial fluid composition on drug delivery vehicles, which is vital to understand and predict pharmacokinetic profiles and behaviors. The aim of our study was therefore to examine the influence of the hard protein coronas on small, cationic NPs subjected to OA synovial fluid or RA synovial fluid, as well as the more frequently used fetal calf serum (FCS) to understand how factors such as size and charge impact the formed coronas and leverage NP uptake in biologically relevant models.

Methods

Materials and Reagents

Ethylenediamine core amino-terminated PAMAM dendrimer Generation 5, methoxypolyethylene glycols (mPEG) 350 and 5000, 4-(Dimethylamino)pyridine (DMAP) ≥ 99 %, PMA, 4-nitrophenyl

chloroformate (4-NPC) 97 %, fluorescein isothiocyanate isomer I, resazurin sodium salt, and sodium phosphotungstate were purchased from Sigma-Aldrich (Munich, Germany).

DPBS (1X) without calcium and magnesium, dichloromethane, dimethyl sulfoxide, deuterium oxide, DMEM (Dulbecco's Modified Eagle's Medium), RPMI 1640 (Roswell Park Memorial Institute), FCS, GlutaMAX, and Pierce BCA protein assay kit were all purchased from Fisher Scientific (Waltham, USA).

Material Synthesis

PEGylation was performed using the methods of Zhao et al.[7] and Geigner et al.[8]. Briefly, mPEG was activated using 4-NPC, dried, purified, and dissolved in DMSO. PAMAM G5 solution (1.585 mM) was diluted using $NaHCO_3$ to maintain pH 8. Mixtures were combined at the stochiometric ratio of 1:3 to achieve ~2% surface PEGylation and allowed to react stirring for 24h at room temperature. Product was dialyzed, dried and stored in the -20°C freezer until further use.

PEGylated PAMAM compounds (NP_0, NP_{350}, NP_{5000}) were dissolved in PBS (pH=7.4) at 5 mg/mL and were allowed to react with fluorescein isothiocyanate isomer I (FITC) in acetone at 1:5 molar ratio respectively. The reaction was carried on in the dark for 12 h, stirring at room temperature. The samples were dialyzed, lyophilized and set at the concentration of 30 μM in PBS (pH=7.4). Products were confirmed by ^1H nuclear magnetic resonance spectroscopy. Samples were solubilized in D2O, recorded using Agilent VnmrS spectrometer at 400 MHz and analyzed by MestReNova version 14.1.1.

Material Characterization

Fluorescence signal was quantified using a CLARIOstar Plus (BMG Labtech, Offenburg, Germany) microplate reader set to detect FITC (λ_{ex} 483/14 nm/ λ_{em} 530/30 nm). Briefly, all FITC-labelled NPs were dissolved in methanol, diluted with PBS to a final concentration of 2 μg/mL, and compared to FITC standard curve. Labelling efficiency was calculated as a proportion of FITC weight to the weight of PAMAM- (0%; 2%-350; 2%-5000) mPEG-FITC in the solution.

NPs (15 μM, pH 6) were briefly sonicated and dropwise placed on a 3 mm holey carbon film coated copper grid (Ted Pella, Inc., Redding, California), stained with 4 % sodium phosphotungstate and allowed to air-dry at room temperature. Images were obtained using Orius CCD camera mounted on

FEI Tecnai T20 transmission electron microscope at 200kV. NP-protein corona samples were prepared as described above with an addition of 1 % trehalose to the 4 % sodium phosphotungstate staining solution. NP size was also assessed using dynamic light scattering (DLS) Zetasizer Nano ZS system (Malvern Instruments, UK). Size of the NPs was measured using disposable semi-micro-UV cuvettes (VWR, Leuven, Belgium), while for zeta potential measurements folded capillary zeta cells (DTS1070, Malvern, UK) were used. Hydrodynamic size and zeta potential is reported as a mean of three runs for each sample size (d.nm) ± s.d (d.nm).

Protein corona isolation/formation

All patients have provided informed consent and the procedure was approved by the Ethics Committee of Gothenburg University (Ethical approval Dnr: 573-07). Synovial fluid samples from 5 (4f/1m**)** RA patients and 4 **(**2f/2m**)** late OA patients were collected during aseptic aspiration of knee joints at the Rheumatology Clinic and at the Orthopaedic Clinic respectively, Sahlgrenska University Hospital, Gothenburg, Sweden.

Patient synovial fluid and control FCS samples were pooled according to the disease profile ($5x10^8$ particles or 2 μg), diluted 1:20 in PBS and mixed with 30 μM solution of PAMAM- (0 %; 2 % -350; 2 % -5000) mPEG-FITC (1:1, v/v). The samples were incubated at 37 °C while shaking for 1 h. Particles were subsequently spun down at 15,000 x g for 15 minutes, washed three times with chilled PBS. The particles with adhered hard protein coronas were resuspended to the final concentration of 1 μg/mL ($2.5x10^8$ particles/mL).

Protein content in the supernatant of the explants was assessed using a Pierce BCA protein assay kit according to manufacturer's instructions. Briefly, the explant study supernatants were mixed with working reagent, incubated at 37 °C, and measured at room temperature at 562 nm wavelength. The experiments were performed in triplicates independently 3 times, n= 4-9.

Biological interactions with NPs

Porcine cartilage tissues were obtained from the Experimental Biomedicine animal facilities under the 3R principle (Gothenburg, Sweden). The specimens entailed unexposed articular joints with femur and tibia still intact of the 3-6-month pigs. Explants were extracted at the femoral and tibial condyle cartilage using biopsy punchers (d= 4 mm) (Kai Medical, Honolulu, USA) and trimmed (~2 mm) to exclude

subchondral bone. Explants were frozen in PBS with 1 % 10,000 U/mL Penicillin, Streptomycin (Gibco) and protease inhibitors (Roche, Switzerland). When thawed or freshly introduced to culture, explants were allowed to equilibrate in DMEM (without phenol red, supplemented with 25 mM HEPES) overnight before the experiment. To quantify FITC-labelled NP uptake into the cartilage, explants were weighed to ensure uniformity before the experiments were started. 100 µL of 30 µM NP_0, NP_{350}, or NP_{5000} - protein corona solutions were administered to the designated explants and incubated for 4 or 24 hours (final NP concentration 12 µM). Each explant condition was performed in triplicates and repeated independently three times. To visualize NP uptake, 24h cartilage explants were fixed in 2% paraformaldehyde, sliced in half and cut along the sagittal plane from the center, stained with DAPI and imaged using Nikon Ti2 inverted microscope with a 20x objective. Images were obtained using ImageJ software.

Cellular studies were performed in a similar manner utilizing Tc28a2 chondrocyte cell line (gift from Dr. Cronstein's lab at NYU Langone, USA) and U937 monocyte cell line (Sigma-Aldrich). The cell experiments were performed under serum-free conditions in DMEM or RPMI respectively. The cells were seeded at $1x10^5$ cells/well in a 48-well plate, incubated with the particles at the indicated timepoints, and washed three times in FACS buffer. Flow cytometry analysis was performed using Guava EasyCyte 8HT (Millipore, Darmstadt, Germany). The FITC was excited by a 488 nm laser, and fluorescence was detected through a 525/30 nm filter. Obtained data was gated to include only single, live cells (after FSC/SSC exclusion of dead cells, >5000 cells) with acquisition range of 5000-10000 cells. The mean cellular uptake of FITC-labeled NPs was estimated as the average fluorescence intensity of all cells within the gate. The data was collected in 1-3 independent experiments and is represented as the means with SD, n=3-4. All flow cytometry data was analyzed and visualized using FlowJo software V10.

Proteomic Analysis

NPs with isolated, hard protein coronas were pelleted, frozen using liquid nitrogen and submitted to the Proteomics Core Facility (Gothenburg, Sweden). Briefly, proteins were digested into peptides using MS-grade trypsin and analyzed by nanoscale liquid chromatography-tandem mass spectrometry LC MS/MS. MS scans were performed in the Orbitrap. Mascot search engine was used to match the

discovered peptide sequences against SwissProt human and bovine protein database using Proteome Discoverer. Data was analyzed using label free quantification (LFQ) method and the protein false discovery rate was set to 1 %. To elucidate the molecular functions and classifications of the significant proteins, enrichment analysis was performed using Gene Ontology (GO) based PANTHER classification system. Synovial fluid samples were matched to human (*Homo sapiens*), while FCS samples were matched to the bovine (*Bos taurus*) databases.

Statistics

Data is presented as mean values ± SD unless otherwise indicated. Statistical analyses were performed using GraphPad Prism (GraphPad Software) version 9.0.2. Shapiro–Wilk test was used to assessed data normality. When comparing two groups, paired t-tests were used to elucidate significance (cartilage uptake studies). Multiple comparison analysis was performed using two-way ANOVA with Tukey's post hoc test. p values <0.05 were considered statistically significant, where * = $p \leq 0.05$, ** = $p \leq 0.01$, *** = $p \leq 0.001$, **** = $p \leq 0.0001$. Statistical and differential analyses for proteomic studies were performed in R (R Foundation for Statistical Computing), using LIMMA, DEP, and ComplexHeatmap R packages. To account for inconsistencies and skewness in the obtained data, data was analyzed using the Mann Whitney Wilcoxon test followed by the Benjamini–Hochberg multiple hypothesis correction. Significance threshold was set for the adjusted p values of <0.05 and ratio change of >1.5 fold.

RESULTS

MATERIAL COMPOSITION AND CHARACTERIZATION

To compare the effect of the synovial fluid protein corona formation and its influence on NP uptake into tissue and cells, a panel of three NP candidates with distinct characteristics based on charge and surface chemistry composition was formulated. The panel consisted of having no PEG, NP_0, short PEG chains, NP_{350}, or long PEG chains NP_{5000} (Figure S1). The size of the NPs were assessed by TEM and DLS and confirmed the expected theoretical sizes (PAMAM G5 = 5.4 nm) (Figure 1A and B). NP_0 measured 7.2 nm ± 2.8 nm, with a slight increase in size for NP_{350} modification, 7.8 nm ± 2.5 nm, and

the largest size as expected for NP_{5000} modification, 11.0 nm ± 4.4 nm. Similarities between NP_0 and NP_{350} were also seen in zeta potential measurements where recorded values were +17.0 mV ± 1.78 mV and +16.0 mV ± 1.95 mV respectively, while NP_{5000} exhibited a lower value of +4.0 mV ± 2.57 mV (Figure 1C). Similar fluorescence intensity profiles for all NPs allowed the FITC probe to be utilized as NP tracker for the biological assays (Figure 1D). Cytotoxicity of the NPs was evaluated on three different cell types including mouse fibroblast (L929), human chondrocyte (Tc28a2), and monocyte (U937) cell lines due to their varied sensitivity. Optimal dosage for biological studies was determined at concentrations ranging from 100 μM to 12.5 μM (Figure S2). Concentrations at which cell viability fell below 70% threshold were regarded as toxic. We observed cellular tolerance to the NPs at concentrations below 50 μM, where NP_{5000} was the most tolerated among the all the tested cell types. Interactions with protein-rich aqueous environments naturally increased the size of the NPs due to protein adherence and hard corona formation (Figure S3A). NP-protein complexes also mediated a negative charge shift in zeta potential under all protein conditions for all NPs (Figure S3B). Synovial fluid derived coronas yielded similar zeta potential results ranging from -13.9 mV ± 1.4 mV (NP_{5000}) to -15.7 mV ± 1.6 mV (NP_0) for OA and from -12.9 mV ± 1.2 mV (NP_{5000}) to -15.5 mV ± 1.2 mV (NP_0) for RA. Meanwhile, FCS condition ranged from -9.4 mV ± 4.1 mV (NP_0) to -10.5 mV ± 3.0 mV (NP_{5000}). Protein concentration assessment revealed differences based on the protein source but did not display any significance based on NP surface chemistry (Figure S3C).

Cartilage Uptake Studies of Hard Protein Corona-Coated NPs

Reduction in the fluorescence signal over time suggested that NP candidates were able to interact with the viable cartilage. All candidates (NP_0, NP_{350} NP_{5000}) subjected to PBS (no protein condition) displayed a significant uptake ($p = 0.0002$, 95% CI = -11.28, -5.77; $p = 0.0002$, 95% CI =-9.84, -4.82; $p = 0.0160$, 95% CI = -10.45, -1.50) after 24h (Figure 2A). However, hard protein corona-decorated NPs displayed a difference depending on the protein source. NP_0 displayed a significant change in fluorescence only in RA condition ($p = 0.0271$, 95% CI = -12.59, -1.03) (Figure 2B), while NP_{350} revealed significant changes in OA ($p = 0.0189$, 95% CI = -6.58, -0.79) and FCS ($p = 0.0068$, 95% CI

= -12.59, -3.34) conditions (Figure 2C). NP_{5000} proved to be the most versatile candidate as it displayed significant changes in fluorescence and subsequent uptake into cartilage in OA ($p = 0.0069$, 95% CI = -14.27, -3.29), RA ($p = 0.0296$, 95% CI = -11.33, -0.80), and FCS ($p = 0.0345$, 95% CI = -12.37, -0.6313) conditions. NP ability to associate with cartilage tissue was further supported by explant imaging after 24h (Figure 2F).

Particle Uptake by Chondrocytes and Monocytes

NP uptake under no protein conditions revealed the highest uptake in both chondrocytes and monocytes regardless of NP surface modification. Interestingly, we observed a decline at 10h time point for all NPs in both cell types that returned to high uptake levels when measured at 24h. Conversely, NP-corona complex uptake ascended at the 10h time point in chondrocytes. NP_0 resulted in the high uptake in chondrocytes, 81.2 % ± 4.2 %, (Figure 3A) at 10h and monocytes, 84.0 % ± 8.8 %, (Figure 3D) at 2h after subjected to FCS followed by RA and OA respectively. Similarly, NP_{350} resulted in the highest uptake under FCS conditions in both chondrocytes, 82.1 % ± 5.9 %, (Figure 3B) and monocytes, 72.1 % ± 17.9 %, after 10h (Figure 3E). In chondrocytes, OA condition resulted in the highest uptake, 55.7 % ± 3.7 %, at 10h (Figure 3C), while in monocytes FCS condition was taken up the most after 30min, 83.9% ± 21.7 % (Figure 3F).

Characterization of Hard Protein Corona-Coated NPs

GO molecular function analysis provided a general overview of OA, RA, and FCS condition differences illustrating functional similarities despite FCS proteins arising from a different animal species (Figure 4A, B, C). Proteins that have a role in binding or possess catalytic activity constituted a large part of the hard protein corona found on all NPs. Protein classification analysis revealed that in the synovial fluid samples, protein activity binding modulators such as C3, C4BPA, C5, ITIH1, ITIH2, ITIH4, SERPINA3, ARF4, HRG, GFA, HSPB1, and others composed the largest part of the differentially abundant proteins (Figure 4D and E) comprising of 26 % and 18 % of the total significant protein count in OA and RA, respectively. In contrast, the largest group of proteins in FCS samples were classified as protein modifying enzymes and included 25 % of the significant proteins, followed by cytoskeletal proteins which comprised 17 % of the total significant protein count (Figure 4F).

The most abundant proteins identified in our synovial fluid samples included albumin, lubricin, fibronectin, inflammation associated proteins, and numerous apolipoproteins. The high abundance of components such as myeloperoxidase, complement proteins such as C1s, C3, C4a/b, C9, hemoglobin subunit beta confirmed the inflammatory state, as well as the findings of various immunoglobulins. ECM associated proteins included inter-alpha-trypsin inhibitor heavy chains, cartilage acidic protein 1, cartilage oligomeric matrix protein, alpha-2-HS-glycoprotein were also located. Additionally, we discovered other proteins which take part in various cell processes and protein transport such as coagulation factor heparin cofactor 2, and prothrombin, actin-binding gelsolin, histone components, and others.

Most abundant proteins found under FCS conditions correlated with soem of the proteins found in the synovial patient samples. Similarities between the synovial fluid and FCS included albumin, complement factors, fibrinogen, inter-alpha-trypsin inhibitor heavy chains, and various apolipoproteins. Common differential proteins between OA and RA included COMP, ITIH1, ITIH2, and SIGLEC5. While these proteins were abundant on the NP_{350} particle, abundance was not as prominent on the NP_{5000}. For OA, the NP_0 showed a similar profile to NP_{5000} with upregulated abundances seen in the proteins involved in the protein transport such as ARF4, ACAP1, RP2 (Figure 5A). NPs with RA-derived coronas were abundant in EMC8, GYS2, H2BC3, TOLLIP (Figure 5 B). NPs with proteins from FCS showed distinct differential abundances for a variety of proteasome subunits (Figure 5 C), in particular with multiple members of PSMB and PSMA families.

DISCUSSION

The nature of the intrinsic biological environment is an important consideration that often is neglected in many drug delivery vehicle studies[9]. Our study addressed this issue by evaluating three types of differentially PEGylated NP, NP_0, NP_{350}, NP_{5000}, and the effects of their interactions with synovial fluids from patients with RA and OA, and FCS on cartilage tissue and cellular uptake.

Our results showed a small size and zeta potential variation between non-PEGylated NP_0 and PEGylated NP_{350} likely due to a small degree of surface conjugation as well as short PEG chains of NP_{350}. NP_{5000} differed from the NPs by slightly larger size as well as lower yet still positive zeta potential arising from

longer, free moving PEG chains in the aqueous environment. Intrinsically cationic PAMAM NPs were engineered to exhibit ~ 2% surface PEGylation to preserve the positive charge, enable distinct surface chemistry, yet avoid cytotoxicity associated with highly cationic NPs. We confirmed the biocompatibility of our NPs on 3 different cell lines including fibroblast L929, a standard proposed by FDA for toxicological studies[10], and cartilage relevant chondrocyte, Tc28a2, and monocyte, U937, cell lines. NP_{5000} proved to be the most tolerated among the different cell types, supporting the effect and importance of PEGylation as a strategy for enhancing biocompatibility in drug delivery systems. Labelling efficiency of NPs was equivalent, thus allowing the NP tracking via FITC fluorescence signal in biological studies.

Protein biocorona formation resulted in a size increase and a negative zeta shift for all NPs-corona complexes, likely arising from the electrostatic interactions between negatively charged proteins present in the synovial fluid and FCS. We found the highest concentration of adhered protein from RA condition, followed by FCS, and OA.

Despite the size, charge change, and amount of adhered protein, we observed the interaction with cartilage in all NPs regardless of subjected protein condition. However, the rate of the uptake into the tissue was dependent on the surface chemistry of the NPs as well as the subsequent protein corona formation. NP_0 exhibited a significant change after 24h when subjected to RA synovial fluid, while for NP_{350} significance was detected when subjected OA and FCS conditions. NP_{5000} displayed a significant change in all protein conditions, thus suggesting its versatile use for FCS, RA, and, in particular, OA applications. These results indicate that the protein presence and identity have major implications for translational cartilage studies with NP-based drug delivery vehicles. This is especially evident from the confocal images, where the naked NPs are distributed deeply into the cartilage, while the NPs with the protein coronas seems to attach to the surface.

For treatments aiming to target joints, it is important not only to consider the tissues but also the cellular uptake. The phagocytic clearance of particles is even more relevant in the inflammatory phase, especially for autoimmune diseases such as RA which has an overactivated immune system.

Chondrocyte and monocyte lines were chosen to reflect the key cells present in the joint space, directing the outcomes of administered therapies[11–13]. Cellular uptake of NPs is highly influenced by the hard

protein corona, especially in their interactions with the immune system[14]. As increased PEGylation results in stealth properties and avoidance of monocyte clearance, this data suggests that the NP_{5000} managed to avoid cellular uptake, in line with previous studies on PEGylation[15], while FCS-derived biocoronas mediated the highest cellular uptake. NP5000, however, exhibited the highest degree of uptake under OA conditions. As avoiding uptake and clearance by monocytes are desirable properties for NPs, the NP_{5000} would continue to hold promise as a nanocarrier design for OA applications. It is important to assess the capacity of drug delivery vehicles to enter chondrocytes, as many drugs aim to alter the function of these ECM-producing cells. Our results suggest that using common lab reagents such as FCS may overestimate the actual cellular uptake of NPs when compared to local conditions. Another consideration and the limitation of our study is the dynamic environment of the synovial fluid as the movement of the join affects the diffusion and clearance rate of drug delivery agents[16].

Based on previous proteome studies in late stage OA synovial fluid, we anticipated to detect an abundance of proteins associated with joint damage such as ECM proteins, proteins involved in complement cascade, coagulation, and an acute immune response [17]. In total, we identified 52, 58, and 59 statistically significant differentially expressed proteins among the NPs for OA, RA, and FCS conditions, respectively. We further determined the significant protein differences between the NP and the corresponding protein conditions revealing the importance of the protein environment. Patient synovial fluids were characterized by a significant differential expression proteins such as TOM1 in OA, and TOLLIP in RA. Literature has recently linked TOM1 protein with endosomal transport, impaired autophagy, and immune response, thus linking TOM1 to pathologies such RA and OA[18,19]. Differential adherence of proteins such as TOM1 and TOLLIP might explain the differences seen in biological uptake studies. TOM1 represents an interesting candidate that could direct NP chondrocyte uptake, as this protein was found mostly abundant on the NP_{5000} and is responsible for recruiting clathrin and driving endosomal cellular uptake and could explain the significance in the cartilage explant uptake for both OA and RA[20]. Interestingly, TOLLIP has been reported to associate with the previously mentioned TOM1 protein, thus together they may direct NP uptake into the cells via endocytic pathways[20,21]. The role of other differentially abundant proteins is yet to be determined in context of NP cellular uptake. Finally, we were able to demonstrate the specificity of certain proteins such as COMP

and ITIH1/2 to NP_{350} in both RA and OA conditions, suggesting that the surface chemistry of the NP affects protein corona composition. Our study is in line with previous research emphasizing the effect of biologically rich environments such as serum and plasma and their effect on establishing the biological NP identity and its impact for the therapeutic translation.

ACKNOWLEDGEMENTS

This work was supported by Chalmers Technical University, its Excellence Initiative Nano, and Area of Advanced Health. The authors acknowledge further financial support from the Kristina Stenborg foundation, the foundation for Sigurd and Elsa Goljes Minne, Apotekare Hedbergs Foundation, and the King Gustav V's 80 years' foundation.

AUTHOR CONTRIBUTIONS

UvM and A.S designed the studies. UvM synthesized the polymers, conducted the in vitro and ex vivo studies and performed analysis. G.E conducted the NMR studies and analysis. T.S and L.R performed in vitro assays and analysis. A.K.H.E provided patient samples and helped with data interpretation. UvM and A.S wrote the manuscript with contributions from all authors, who also approved the final version.

DECLARATION OF COMPETING INTERESTS

Authors declare no competing interests.

REFERENCES

(1) Glyn-Jones S, Palmer AJR, Agricola R, Price AJ, Vincent TL, Weinans H, et al. Osteoarthritis. Lancet 2015, 386 (9991), 376–387. https://doi.org/10.1016/S0140-6736(14)60802-3.

(2) Bajpayee AG, Grodzinsky AJ. Cartilage-Targeting Drug Delivery: Can Electrostatic Interactions Help? Nat. Rev. Rheumatol. 2017, 13 (3), 183–193. https://doi.org/10.1038/nrrheum.2016.210.

(3) Bajpayee AG, Scheu M, Grodzinsky AJ, Porter RM. Electrostatic Interactions Enable Rapid Penetration, Enhanced Uptake and Retention of Intra-Articular Injected Avidin in Rat Knee Joints. J. Orthop. Res. 2014, 32 (8), 1044–1051. https://doi.org/10.1002/jor.22630.

(4) Lundqvist M, Cedervall T. Three Decades of Research about the Corona Around Nanoparticles: Lessons Learned and Where to Go Now. Small 2020, 16 (46), 2000892. https://doi.org/10.1002/smll.202000892.

(5) Visalakshan RM, González García LE, Benzigar MR, Ghazaryan A, Simon J, Mierczynska-Vasilev A, et al. The Influence of Nanoparticle Shape on Protein Corona Formation. Small 2020, 16 (25), 2000285. https://doi.org/10.1002/smll.202000285.

(6) Mirshafiee V, Kim R, Mahmoudi M, Kraft ML. The Importance of Selecting a Proper Biological Milieu for Protein Corona Analysis in Vitro: Human Plasma versus Human Serum. Int. J. Biochem. Cell Biol. 2016, 75, 188–195. https://doi.org/10.1016/j.biocel.2015.11.019.

(7) Zhao D, Xu JQ, Yi XQ, Zhang Q, Cheng SX, Zhuo RX, et al. PH-Activated Targeting Drug Delivery System Based on the Selective Binding of Phenylboronic Acid. ACS Appl. Mater. Interfaces 2016, 8 (23), 14845–14854. https://doi.org/10.1021/acsami.6b04737.

(8) Geiger BC, Wang S, Padera RF, Grodzinsky AJ, Hammond PT. Cartilage-Penetrating Nanocarriers Improve Delivery and Efficacy of Growth Factor Treatment of Osteoarthritis. Sci. Transl. Med. 2018, 10 (469), 1–13. https://doi.org/10.1126/scitranslmed.aat8800.

(9) Berrecoso G, Crecente-Campo J, Alonso MJ. Unveiling the Pitfalls of the Protein Corona of Polymeric Drug Nanocarriers. Drug Deliv. Transl. Res. 2020, 10 (3), 730–750. https://doi.org/10.1007/s13346-020-00745-0.

(10) ISO 10993-5:2009, Biological evaluation of medical devices — Part 5: Tests for in vitro cytotoxicity https://www.iso.org/standard/36406.html.

(11) McInnes IB, Schett G. Pathogenetic Insights from the Treatment of Rheumatoid Arthritis.

Lancet 2017, 389 (10086), 2328–2337. https://doi.org/10.1016/S0140-6736(17)31472-1.

(12) Bosch van den MHJ. Osteoarthritis Year in Review 2020: Biology. Osteoarthr. Cartil. 2021, 29 (2), 143–150. https://doi.org/10.1016/j.joca.2020.10.006.

(13) Moradi B, Rosshirt N, Tripel E, Kirsch J, Barié A, Zeifang F, et al. Unicompartmental and Bicompartmental Knee Osteoarthritis Show Different Patterns of Mononuclear Cell Infiltration and Cytokine Release in the Affected Joints. Clin. Exp. Immunol. 2015, 180 (1), 143–154. https://doi.org/10.1111/cei.12486.

(14) Ju Y, Kelly HG, Dagley LF, Reynaldi A, Schlub TE, Spall SK, et al. Person-Specific Biomolecular Coronas Modulate Nanoparticle Interactions with Immune Cells in Human Blood. ACS Nano 2020, 14 (11), 15723–15737. https://doi.org/10.1021/acsnano.0c06679.

(15) Sivaram AJ, Wardiana A, Alcantara S, Sonderegger SE, Fletcher NL, Houston ZH, et al. Controlling the Biological Fate of Micellar Nanoparticles: Balancing Stealth and Targeting. ACS Nano 2020, 14 (10), 13739–13753. https://doi.org/10.1021/acsnano.0c06033.

(16) Mekheimer KS, Abo-Elkhair RE, Abdelsalam SI, Ali KK, Moawad AMA. Biomedical Simulations of Nanoparticles Drug Delivery to Blood Hemodynamics in Diseased Organs: Synovitis Problem. Int. Commun. Heat Mass Transf. 2022, 130 (December 2021), 105756. https://doi.org/10.1016/j.icheatmasstransfer.2021.105756.

(17) Ritter SY, Subbaiah R, Bebek G, Crish J, Scanzello CR, Krastins B, et al. Proteomic Analysis of Synovial Fluid from the Osteoarthritic Knee: Comparison with Transcriptome Analyses of Joint Tissues. Arthritis Rheum. 2013, 65 (4), 981–992. https://doi.org/10.1002/art.37823.

(18) Roach, TG, Lång HKM, Xiong W, Ryhänen SJ, Capelluto DGS. Protein Trafficking or Cell Signaling: A Dilemma for the Adaptor Protein TOM1. Front. Cell Dev. Biol. 2021, 0, 408. https://doi.org/10.3389/fcell.2021.643769.

(19) KeskitaloS , Haapaniemi EM, Glumoff V, Liu X, Lehtinen V, Fogarty C, et al. Dominant TOM1

Mutation Associated with Combined Immunodeficiency and Autoimmune Disease. npj Genomic Med. 2019 41 2019, 4 (1), 1–7. https://doi.org/10.1038/s41525-019-0088-5.

(20) Katoh Y, Imakagura H, Futatsumori M, Nakayama K. Recruitment of Clathrin onto Endosomes by the Tom1-Tollip Complex. Biochem. Biophys. Res. Commun. 2006, 341 (1), 143–149. https://doi.org/10.1016/j.bbrc.2005.12.156.

(21) Xiao S, Brannon MK, Zhao X, Fread KI, Ellena JF, Bushweller JH, et al. Tom1 Modulates Binding of Tollip to Phosphatidylinositol 3-Phosphate via a Coupled Folding and Binding Mechanism. Structure 2015, 23 (10), 1910–1920. https://doi.org/10.1016/j.str.2015.07.017.

Figures

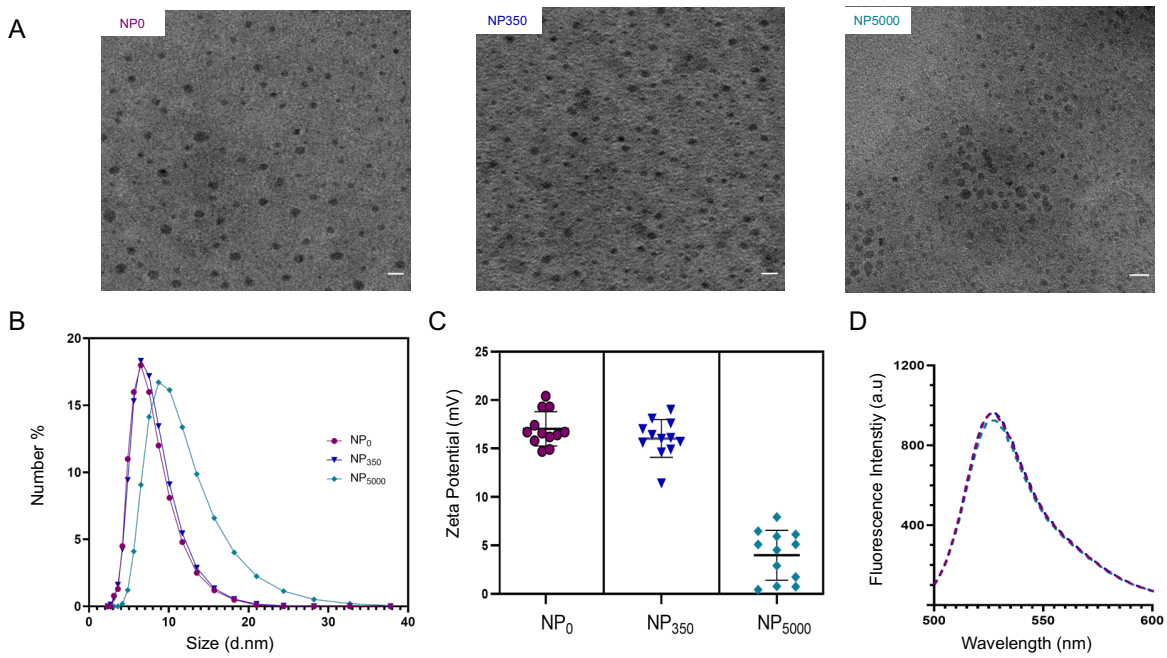

Figure 1.

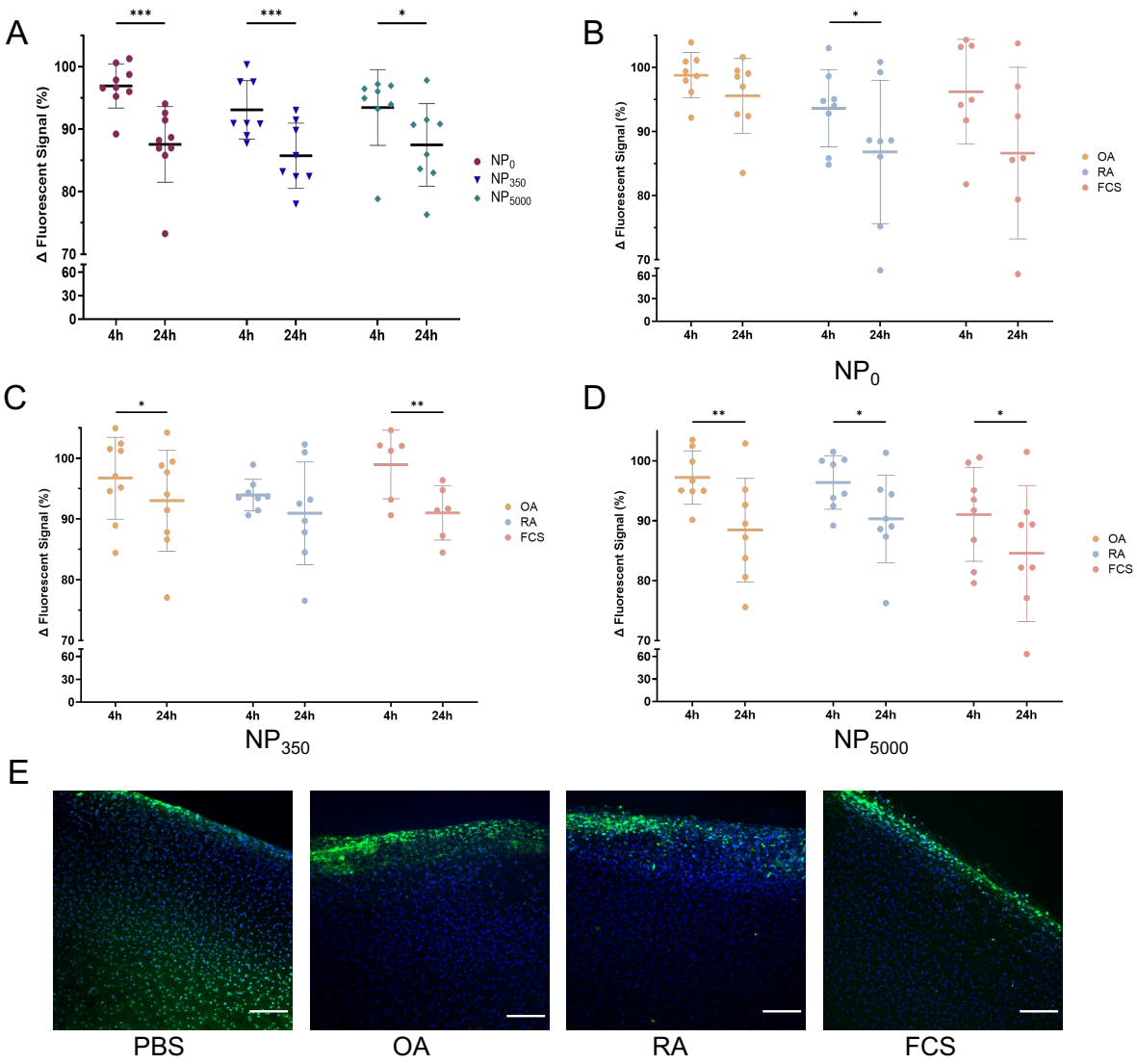
A
B
C
D
E
Δ Fluorescent Signal (%)
4h
24h
NP0
NP350
NP5000
OA
RA
FCS
PBS

Figure 2.

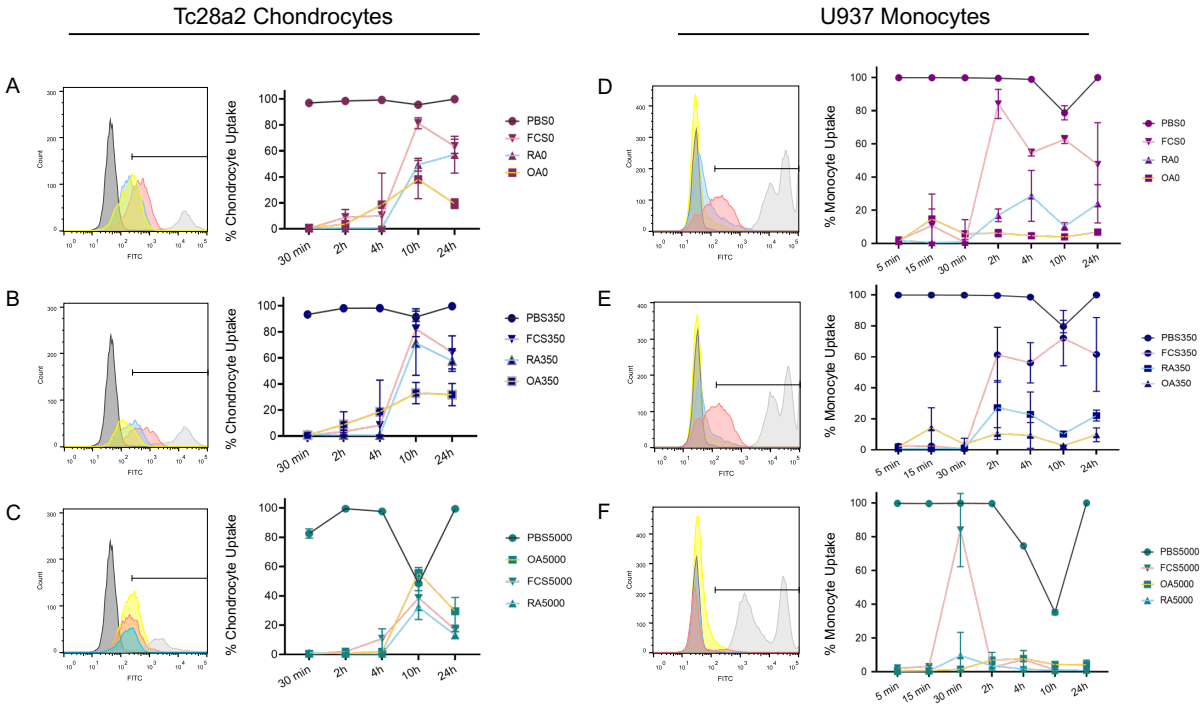
Tc28a2 Chondrocytes
U937 Monocytes
A
B
C
D
E
F
% Chondrocyte Uptake
% Monocyte Uptake
FITC
Count
30 min
2h
4h
10h
24h
5 min
15 min
PBS0
FCS0
RA0
OA0
PBS350
FCS350
RA350
OA350
PBS5000
FCS5000
OA5000
RA5000

Figure 3.

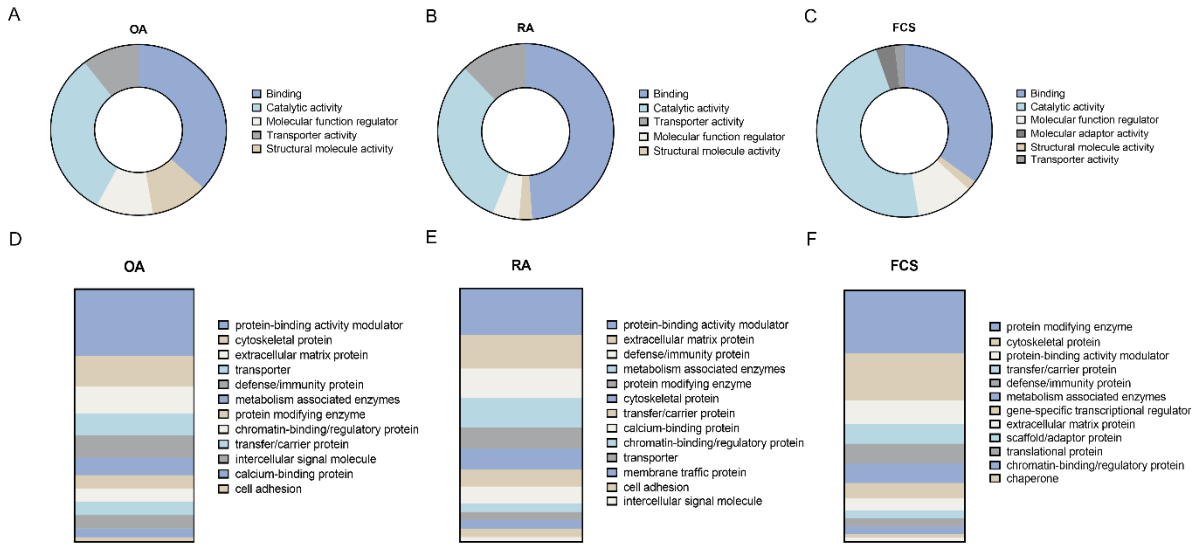
A
OA
Binding
Catalytic activity
Molecular function regulator
Transporter activity
Structural molecule activity
B
RA
Binding
Catalytic activity
Transporter activity
Molecular function regulator
Structural molecule activity
C
FCS
Binding
Catalytic activity
Molecular function regulator
Molecular adaptor activity
Structural molecule activity
Transporter activity
D
OA
protein-binding activity modulator
cytoskeletal protein
extracellular matrix protein
transporter
defense/immunity protein
metabolism associated enzymes
protein modifying enzyme
chromatin-binding/regulatory protein
transfer/carrier protein
intercellular signal molecule
calcium-binding protein
cell adhesion
E
RA
protein-binding activity modulator
extracellular matrix protein
defense/immunity protein
metabolism associated enzymes
protein modifying enzyme
cytoskeletal protein
transfer/carrier protein
calcium-binding protein
chromatin-binding/regulatory protein
transporter
membrane traffic protein
cell adhesion
intercellular signal molecule
F
FCS
protein modifying enzyme
cytoskeletal protein
protein-binding activity modulator
transfer/carrier protein
defense/immunity protein
metabolism associated enzymes
gene-specific transcriptional regulator
extracellular matrix protein
scaffold/adaptor protein
translational protein
chromatin-binding/regulatory protein
chaperone

Figure 4.

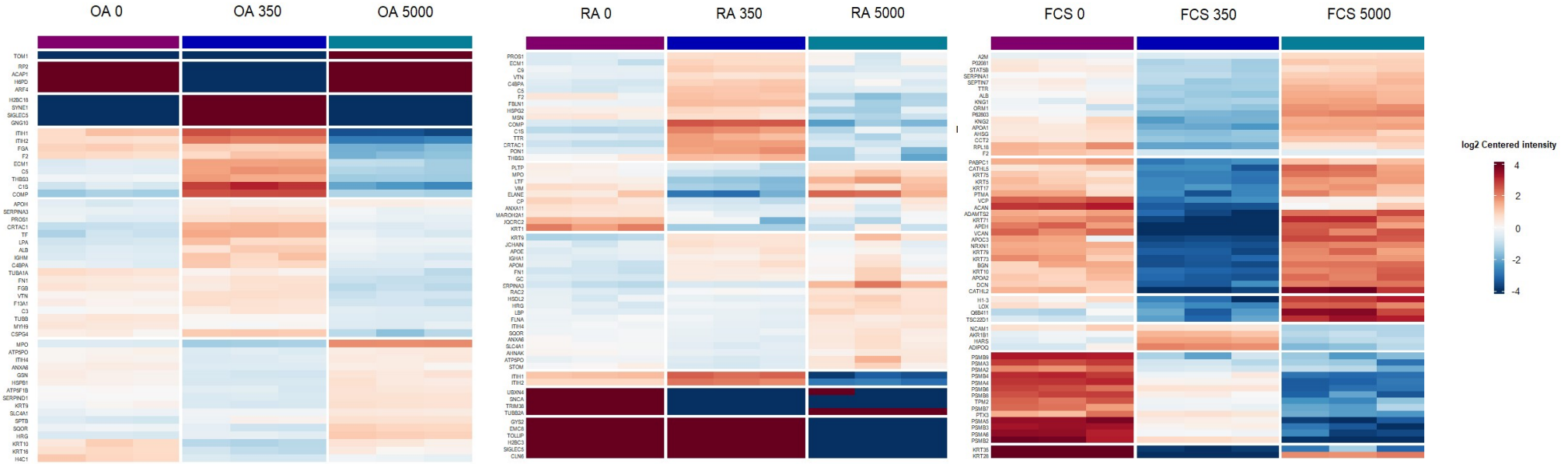

Gene	Protein	log2FC 0	log2FC 350	log2FC 5000
ARF4	ADP-ribosylation factor 4	6,66	-13,3	6,64
ACAP1	Arf-GAP with coiled-coil, ANK repeat and PH domain-containing protein 1	6,56	-11,7	5,16
COMP	Cartilage oligomeric matrix protein	-1,39	2,65	-1,26
C1S	Complement C1s subcomponent	-0,64	2,97	-2,33
H6PD	GDH/6PGL endoplasmic bifunctional protein	6,01	-12,6	6,57
GNG10	Guanine nucleotide-binding protein G(I)/G(S)/G(O) subunit gamma-10	-6,67	13,3	-6,67
H2BC18	Histone H2B type 2-F	-5,91	11,8	-5,91
ITIH1	Inter-alpha-trypsin inhibitor heavy chain H1	1,05	2,51	-3,56
ITIH2	Inter-alpha-trypsin inhibitor heavy chain H2	0,69	2,07	-2,75
MPO	Myeloperoxidase	-0,54	-1,35	1,89
SYNE1	Nesprin-1	-6,01	12	-6,01
RP2	Protein XRP2	5,27	-11,1	5,86
SIGLEC5	Sialic acid-binding Ig-like lectin 5	-5,65	11,3	-5,65
TOM1	Target of Myb protein 1	-6,49	-6,49	13

Gene	Protein	log2FC 0	log2FC 350	log2FC 5000
SNCA	Alpha-synuclein	12,4	-6,22	-6,22
COMP	Cartilage oligomeric matrix protein	-0,68	2,51	-1,82
CLN6	Ceroid-lipofuscinosis neuronal protein 6	6,48	5,26	-11,7
TRIM38	E3 ubiquitin-protein ligase TRIM38	11	-5,52	-5,52
EMC8	ER membrane protein complex subunit 8	6,94	6,83	-13,8
GYS2	Glycogen [starch] synthase, liver	6,04	6,96	-13
H2BC3	Histone H2B type 1-B	7,46	6,3	-13,8
ITIH1	Inter-alpha-trypsin inhibitor heavy chain H1	1,2	2,35	-3,54
ITIH2	Inter-alpha-trypsin inhibitor heavy chain H2	0,84	2,06	-2,89
ELANE	Neutrophil elastase	0,63	-2,63	2
SIGLEC5	Sialic acid-binding Ig-like lectin 5	8,02	4,64	-12,7
TOLLIP	Toll-interacting protein	7,51	6,79	-14,3
TUBB2A	Tubulin beta-2A chain	5,96	-13,8	7,8
UBXN4	UBX domain-containing protein 4	11,1	-8,25	-2,82

Gene	Protein	log2FC 0	log2FC 350	log2FC 5000
ADAMTS2	A disintegrin and metalloproteinase with thrombospondin motifs 2	1,52	-3,88	2,36
ACAN	Aggrecan core protein	3,04	-3,44	0,40
APOC3	Apolipoprotein C-III	1,02	-3,66	2,64
CATHL2	Cathelicidin-2	1,27	-4,8	3,53
KRT35	Keratin, type I cuticular Ha5	6,72	-4,23	-2,49
KRT28	Keratin, type I cytoskeletal 28	4,51	-6,46	1,94
KRT71	Keratin, type II cytoskeletal 71	1,85	-4,56	2,72
Q6B411	Lysozyme C, milk isozyme	-0,79	-2,55	3,34
PSMA5	Proteasome subunit alpha type-5	3,58	0,24	-3,82
PSMB2	Proteasome subunit beta type-2	3,65	0,73	-4,38
PSMB3	Proteasome subunit beta type-3	3,38	0,19	-3,58
PSMB4	Proteasome subunit beta type-4	3,01	0,02	-3,03
TSC22D1	TSC22 domain family protein 1	-0,71	-2,49	3,19
VCAN	Versican core protein	2,2	-4,54	2,35

Figure 5.

Figure Legends

Figure 1. PAMAM-PEG$_x$-FITC NP characterization. (A) The sizes of the NPs were assessed with TEM in a 15 μM PBS suspension at pH=6, scale bar = 10 nm. (B, C) The hydrodynamic diameter of the particles was measured at 30 μM, neutral pH environment and the values were extracted based on the size distribution by volume, and zeta potential was quantified using DLS. (D) Green fluorescence FITC signal was measured and quantified λ= ex. 483/14 nm, λ= em. 530/30 nm by a fluorescence spectrophotometer.

Figure 2. Investigation of PAMAM-PEG$_x$-FITC NP uptake to the cartilage tissue explants. (A) 30 μM of NPs were administered to cartilage explants and incubated for 4 h or 24 h. FITC signal was detected using a fluorescence spectrophotometer and NP uptake into the cartilage tissue was assessed after T4 or T24 hours and normalized to its correspondent T0 signal. Each NP suspension was subjected to three different protein abundant conditions – OA = pooled OA patient synovial fluid (2f/2m); RA = pooled RA patient synovial fluid (4f/1m); FCS = fetal calf serum. The influence of the formed hard protein corona on cartilage uptake was compared for NP_0, NP_{350}, and NP_{5000}, respectively (B,C,D). (E) Representative confocal images of cartilage uptake of NP_0 particles after 24h. Nanoparticles appear as green, while DAPI was used to allow visualization of the chondrocytes in the tissue. Scale bar indicates 50 μm. Data is representative of 3 independent experiment repeats, n= 4-9. Error bars represent standard deviations, while the significance was assessed using paired t-tests.

Figure 3. Assessment of PAMAM-PEG$_x$-FITC nanoparticle uptake in chondrocytes (A, B, C) and monocytes (D,E,F) at the indicated timepoints. NPs were preincubated with either PBS or OA, RA, or FCS for 1 hour before washing. % uptake refers to the proportion of cells with

positive fluorescence above background control, stemming from FITC-labelled NPs analyzed by flow cytometry. Flow cytometry histograms represent association with NP_0 (A,D), NP_{350} (B,E) or NP_{5000}, where PBS treated particles are depicted in light grey, FCS in pink, RA in blue, OA in yellow and the negative control is depicted in dark grey (C,F). Data is shown as the mean and SD of n=3-4, 1-3 independent experiments.

Figure 4. Pathway enrichment analysis for the differential protein abundances on the coronas detected in the panel of PAMAM-PEGx-FITC NPs. (A,B,C) PANTHER based analysis revealed molecular function of the identified proteins in human patient OA synovial fluid, human patient RA synovial fluid), and bovine fetal calf serum (FCS) samples, respectively. (D,E,F) To further compare the difference between the detected proteins on the NP coronas, protein classification was also elucidated for the OA , RA , and FCS samples respectively using the same analysis comparison.

Figure 5. (A, B, C) Heat maps of the differentially expressed significant proteins associated with individual protein coronas on NP_0, NP_{350}, and NP_{5000} exposed to late-stage OA synovial fluid (52) (A, B, C), RA synovial fluid (58), or commercially available FCS (59) respectively. The red and blue color scheme indicates high and low abundance of LFQ intensities represented as log2FC. The tables below summarize the top 14 differentially expressed proteins among the NP groups.